

ALIGNING VISUAL CONTRASTIVE LEARNING MODELS VIA PREFERENCE OPTIMIZATION

Amirabbas Afzali, Borna Khodabandeh *
 {amir8afzali, borna710kh}@gmail.com

Ali Rasekh
 L3S Research Center
 ali.rasekh@l3s.de

Mahyar JafariNodeh
 Massachusetts Institute of Technology, USA
 mahyarjn@mit.edu

Sepehr kazemi
 sepehrkazemi9@gmail.com

Simon Gottschalk
 L3S Research Center
 gottschalk@l3s.de

ABSTRACT

Contrastive learning models have demonstrated impressive abilities to capture semantic similarities by aligning representations in the embedding space. However, their performance can be limited by the quality of the training data and its inherent biases. While Reinforcement Learning from Human Feedback (RLHF) and Direct Preference Optimization (DPO) have been applied to generative models to align them with human preferences, their use in contrastive learning has yet to be explored. This paper introduces a novel method for training contrastive learning models using Preference Optimization (PO) to break down complex concepts. Our method systematically aligns model behavior with desired preferences, enhancing performance on the targeted task. In particular, we focus on enhancing model robustness against typographic attacks, commonly seen in contrastive models like CLIP. We further apply our method to disentangle gender understanding and mitigate gender biases, offering a more nuanced control over these sensitive attributes. Our experiments demonstrate that models trained using PO outperform standard contrastive learning techniques while retaining their ability to handle adversarial challenges and maintain accuracy on other downstream tasks. This makes our method well-suited for tasks requiring fairness, robustness, and alignment with specific preferences. We evaluate our method on several vision-language tasks, tackling challenges such as typographic attacks. Additionally, we explore the model’s ability to disentangle gender concepts and mitigate gender bias, showcasing the versatility of our approach.

1 INTRODUCTION

In recent years, Vision-Language Models (VLMs) such as CLIP (Radford et al., 2021) have revolutionized downstream vision-language tasks like classification (Conde & Turgutlu, 2021), object detection (Zhong et al., 2021), segmentation (Xu et al., 2022), and image generation (Saharia et al., 2022). These models are trained on large-scale web data, such as the 400 million text-image pairs used for training CLIP. However, despite their success, VLMs exhibit several vulnerabilities. For instance, adversarial attacks (Goodfellow et al., 2015; Moosavi-Dezfooli et al., 2016) and backdoor vulnerabilities (Bai et al., 2024; Liang et al., 2024) can lead to erroneous classifications with high confidence. CLIP has also been shown to be vulnerable to typographic attacks, where text within images causes misclassification (Goh et al., 2021). Additionally, biases such as gender and racial bias (Ruggeri & Nozza, 2023; Zhang et al., 2022b; Bolukbasi et al., 2016; Jialu Wang et al., 2021) can be

*Equal contribution.

amplified by these models due to biases in their training datasets. Another dispreferred behavior occurs when models focus on tasks unrelated to the intended objective, as highlighted by (Menon et al., 2022). These challenges underscore the need for alignment methods in large pre-trained models.

Generative models, including Large Language Models (LLMs), have also been widely adopted for solving complex problems across various domains. Examples in the literature include GPT-4 (Achiam et al., 2023), Mistral (Albert Q. Jiang et al., 2023), and LLaMA (Touvron et al., 2023). These models are trained on massive datasets of unlabeled text, learning general language representations. Some of these LLMs require additional Supervised Fine-Tuning (SFT) to specialize for specific tasks using labeled data. However, even with fine-tuning, LLMs can produce outputs that misalign with human values or safety expectations, such as the unreliability of LLMs in autonomous driving (Chen et al., 2024). To mitigate this, alignment techniques are applied, where models are further trained using a reward model that captures human preferences (Stiennon et al., 2022; Ouyang et al., 2022b; Bai et al., 2022). Popular alignment approaches include Reinforcement Learning from Human Feedback (RLHF) (Ouyang et al., 2022b; Christiano et al., 2023) and Direct Preference Optimization (DPO) (Rafailov et al., 2023), both of which extend the capabilities of these models beyond what SFT alone can achieve. These alignment techniques have improved the safety and relevance of LLM outputs by making them more aligned with human preferences.

Alignment methods have been explored in VLMs (Sun et al., 2023; Gallego, 2023; Clark et al., 2023), but to the best of our knowledge, they have not been extensively applied to contrastive learning models like CLIP. In this work, we extend the preference optimization paradigm to non-generative VLMs. Our approach builds on the contrastive learning framework while simultaneously aiming to preserve the pretrained knowledge—a concept known as continual learning (Garg et al., 2024; Wang et al., 2023).

In this work, we extend the preference optimization paradigm to contrastive learning models, focusing on enhancing robustness against typographic attacks and mitigating gender biases. By systematically aligning the model’s behavior with human preferences, we aim to preserve its pretrained knowledge while improving its performance in sensitive areas such as fairness and robustness. The core tasks addressed in this work—mitigating typographic attacks and disentangling gender biases—underscore the versatility of our approach and its potential for improving model alignment in real-world applications. Our contributions are as the following:

- We extend preference optimization methods, originally developed for generative models, to non-generative models, particularly contrastive learning models. This expansion opens new opportunities for improving model alignment in non-generative tasks, preserving the pretrained knowledge of models while optimizing for desired behaviors.
- We propose controlling model behavior by adjusting the singular values of a learnable linear transformation. This allows fine-tuning of specific concepts, like gender, by modulating critical directions in the representation space while preserving overall performance. This method provides precise control and interpretability, enabling flexible post-training adjustments.
- Our experiments demonstrate the usefulness of applying preference optimization in contrastive learning tasks, such as training for robustness against typographic attacks and disentangling gender information from the embedding space, mitigating gender bias, and showcasing its effectiveness in improving model behavior in real-world scenarios.

2 FOUNDATIONS & RELATED WORK

Preference Optimization and RLHF. Reinforcement Learning from Human Feedback (RLHF) aligns model behavior with human preferences by training the model based on feedback from human annotators. In the standard RLHF paradigm, annotators rank model responses. For example, given an input prompt x , a preference inequality might be expressed as $y_l \prec y_w$, meaning response y_w is preferred over response y_l for prompt x . These preferences are structured into datasets $\mathcal{D} = \{(x, y_w, y_l)\}$. The preference modeling often follows energy-based methods like the Bradley-Terry model (Bradley & Terry, 1952), where the probability of preferring y_w over y_l is modeled as below,

where r^* is the ‘‘true’’ reward function underlying the preferences:

$$P^*(y_w \succ y_l | x) = \frac{e^{r^*(x, y_w)}}{e^{r^*(x, y_w)} + e^{r^*(x, y_l)}} = \sigma(r^*(x, y_w) - r^*(x, y_l)). \quad (1)$$

Since obtaining the true reward r^* from a human is impossible, a reward model r_ϕ is learned by approximating the true reward function. This model is optimized by minimizing the negative log-likelihood of the human preference data:

$$\mathcal{L}_R(r_\phi) = \mathbb{E}_{x, y_w, y_l \sim \mathcal{D}}[-\log(\sigma(r_\phi(x, y_w) - r_\phi(x, y_l)))]. \quad (2)$$

Once the reward function is learned, the RL pipeline can be used to improve the generation policy. To prevent significant deviation from the pretrained reference model, a KL-divergence-shaped reward is incorporated, with the RL objective defined as:

$$\max_{\pi_\theta} \mathbb{E}_{x \sim \mathcal{D}, y \sim \pi_\theta} [r_\phi(x, y)] - \beta D_{\text{KL}}(\pi_\theta(y|x) \| \pi_{\text{ref}}(y|x)), \quad (3)$$

where $\beta > 0$ controls the degree of allowed divergence from π_{ref} . Unlike RLHF, which is often slow and unstable due to its reliance on sampling and reinforcement learning, DPO (Rafailov et al., 2024) offers a more efficient and stable alternative by directly defining a loss function and bypassing reinforcement learning, allowing for standard optimization. However, DPO can sometimes overfit to preference datasets. To address this, Identity Preference Optimization (IPO) (Azar et al., 2023b) bypasses the Bradley-Terry modelization and introduces a new loss function to decrease overfitting by controlling the gap between the likelihood ratios of the model and a reference model. Defining the *policy ratio* as below:

$$h_{\pi_\theta}(y_w, y_l; x) = \log \left(\frac{\pi_\theta(y_w|x) \pi_{\text{ref}}(y_l|x)}{\pi_\theta(y_l|x) \pi_{\text{ref}}(y_w|x)} \right). \quad (4)$$

We can now express both the DPO and IPO objectives in terms of this ratio:

$$\mathcal{L}_{\text{DPO}}(\pi_\theta, \pi_{\text{ref}}) = \mathbb{E}_{(x, y_l, y_w) \sim \mathcal{D}} [-\log \sigma(\beta h_{\pi_\theta}(y_w, y_l, x))], \quad (5)$$

$$\mathcal{L}_{\text{IPO}}(\pi_\theta; \pi_{\text{ref}}) = \mathbb{E}_{(x, y_w, y_l) \sim \mathcal{D}} \left[\left(h_{\pi_\theta}(y_w, y_l; x) - \frac{\beta^{-1}}{2} \right)^2 \right]. \quad (6)$$

Additionally, newer methods like Kahneman-Tversky Optimization (KTO) (Kawin Ethayarajh et al., 2024) only require a binary signal of whether an output is desirable or undesirable, making it more practical for many real-world applications:

$$\mathcal{L}_{\text{KTO}}(\pi_\theta, \pi_{\text{ref}}) = \mathbb{E}_{x, y \sim \mathcal{D}} [w(y)(1 - v_{\text{KTO}}(x, y; \beta))], \quad (7)$$

where the weights $w(y)$ depend on whether the outcome is desirable or undesirable, and v_{KTO} adjusts the model based on the reference distribution:

$$v_{\text{KTO}}(x, y; \beta) = \begin{cases} \sigma(r_{\text{KTO}}(x, y) - z_{\text{ref}}) & y \sim y_{\text{desirable}}|x \\ \sigma(z_{\text{ref}} - r_{\text{KTO}}(x, y)) & y \sim y_{\text{undesirable}}|x \end{cases}, \quad w(y) = \begin{cases} \lambda_U & y \sim y_{\text{undesirable}}|x \\ \lambda_D & y \sim y_{\text{desirable}}|x \end{cases},$$

where $z_{\text{ref}} = \mathbb{E}_{x' \sim \mathcal{D}} [\beta D_{\text{KL}}(\pi_\theta(y'|x') \| \pi_{\text{ref}}(y'|x'))]$ and $r_{\text{KTO}}(x, y) = \beta \log \frac{\pi_\theta(y|x)}{\pi_{\text{ref}}(y|x)}$. Further details of mentioned methods are provided in Appendix A. These methods have been widely adopted in training generative models, including diffusion models like Denoising Diffusion Policy Optimization (DDPO) (Black et al., 2024). This work investigates how these methodologies can be applied to contrastive learning-based models. This paper focused on two critical applications: mitigating typographic attacks and addressing biases, such as gender bias in contrastive models like CLIP.

Typographic attacks. Typographic attacks exploit a model’s tendency to prioritize text over visual content, as shown by (Goh et al., 2021), causing CLIP to misclassify images based on misleading text. For example, writing ‘‘cat’’ on an image of a dog could lead CLIP to incorrectly label it as ‘‘an image of a cat’’. This represents a clear example of undesired behavior in CLIP and is an ideal test case for preference optimization. Recent works, such as (Azuma & Matsui, 2023b; Joanna Materzynska et al., 2022; Ilharco et al., 2022), address this shortcoming through various fine-tuning schemes.

Gender bias, task bias, and other inductive biases. Biases such as gender and racial bias (Ruggeri & Nozza, 2023; Zhang et al., 2022b; Bolukbasi et al., 2016; Jialu Wang et al., 2021) are prevalent in vision-language models like CLIP. These models often unintentionally encode and maintain societal biases, leading to skewed predictions that disproportionately affect marginalized groups. Another common issue is task bias, where models may focus on unintended aspects of the task, further amplifying distortions in their outputs.

3 METHODOLOGY

3.1 PROBLEM FORMULATION: CONTRASTIVE LEARNING AS AN MDP

To effectively apply preference optimization to contrastive learning models, we first need to frame the problem within the reinforcement learning paradigm, modeling it as a Markov decision process (MDP). Specifically, we define the contrastive learning task as a one-step MDP, denoted as $\mathcal{M} = (\mathcal{S}, \mathcal{A}, \rho_0, P, R, \gamma)$, where \mathcal{S} is the state space, \mathcal{A} is the action space, ρ_0 is the initial state distribution, P is the transition function, R is the reward function, and γ is the discount factor. Since it is a one-step process, the transition function P and the discount factor γ are unnecessary, as states do not continue beyond the first step. In this setup, the model operates as a retrieval system: the input (either text or image) represents the state $s \in \mathcal{S}$, and the most similar text or image is selected as the action $a \in \mathcal{A}$. Additionally, ρ_0 defines the distribution of initial states, and R represents the reward function.

The policy $\pi_\theta(a|s)$ is defined analogously to the contrastive learning objective, typically using a softmax function over the similarity score $f_\theta(x, y) = \mathcal{I}_\theta(x)^T \mathcal{T}_\theta(y) / \tau$, where $\mathcal{I}_\theta : \mathcal{X}_{\text{image}} \rightarrow \mathbb{R}^d$ and $\mathcal{T}_\theta : \mathcal{X}_{\text{text}} \rightarrow \mathbb{R}^d$ are the encoders for the image and text, respectively. Here, $\mathcal{X}_{\text{image}}$ and $\mathcal{X}_{\text{text}}$ represent the input distributions of images and texts, and d is the dimensionality of the latent space where both image and text representations are embedded. θ represents the model parameters, and τ is the temperature. The action space is chosen from a fixed set of possible outputs $\mathcal{A} = \mathcal{Y} \triangleq \{y_i\}_{i \in \{1, \dots, K\}}$, where K represents the total number of classes. The components of $\mathcal{M}(\mathcal{S}, \mathcal{A}, \rho_0, R)$ are defined as follows:

$$\begin{cases} s \triangleq x \\ a \triangleq y \end{cases}, \quad \begin{cases} \rho_0(s) \triangleq p(x) \\ R(s, a) \triangleq r(x, y) \end{cases}, \quad \pi_\theta(a|s) \triangleq \frac{e^{f_\theta(y, x)}}{\sum_{y_i} e^{f_\theta(y_i, x)}}.$$

This MDP framework can be applied to different tasks and provides flexibility in designing policies. We specifically utilize methods like DPO and KTO due to their implicit reward modeling, which allows for more effective model alignment with desired behaviors.

3.2 PREFERENCE AND REGULARIZATION DATASETS

In our framework, the desired response of the model given an input x (e.g., an adversarial image) is considered the preferred output y_w . This represents the correct or human-aligned response that we aim to optimize for. On the other hand, the dispreferred output y_l refers to the model’s potentially biased response, or the target of an adversarial attack, or an undesirable outcome (such as bias related to gender or other attributes). The model learns to be robust against adversarial attacks or specific biases by comparing these two outputs.

We use two datasets to facilitate this learning:

- **Preference Dataset $\mathcal{D}_{\text{pref}}$:** This dataset contains pairs (x, y_w, y_l) , where y_w is the preferred output and y_l is the dispreferred output. The model learns to differentiate between desired and undesired outcomes through this dataset, improving its robustness against adversarial attacks and biases.
- **Regularization Dataset \mathcal{D}_{reg} :** This dataset consists of clean samples (images or text) without adversarial manipulation. It is used during training to ensure the model retains its accuracy on clean data, enhancing its robustness in general scenarios.

By combining the preference and regularization datasets, the model is trained to align with a specific behavior or be robust against adversarial inputs while maintaining performance on clean data and other downstream tasks.

3.3 PREFERENCE-BASED CONTRASTIVE OPTIMIZATION

Building on the proposed formulation, preference optimization can be effectively applied to contrastive learning models by guiding the optimization process toward desired behaviors. Moreover, we can shape the policy to learn specific behaviors or patterns by defining them as *preferred*. Furthermore, in section 4.3, we highlight a significant advantage of this optimization paradigm as a

fine-tuning method, helping retain the pre-trained knowledge of the model while adapting it to new preferences and support it with experiment results.

Recalling Equation 4, we first focused on policy ratio, $h_{\pi_\theta}(y_w, y_l, x)$ which we can write as the following:

$$h_{\pi_\theta}(y_w, y_l, x) = \left(\log \pi_\theta(y_w|x) - \log \pi_\theta(y_l|x) \right) - \left(\log \pi_{\text{ref}}(y_w|x) - \log \pi_{\text{ref}}(y_l|x) \right) \quad (8)$$

Given that the objective of the model π_θ is to simultaneously increase the probability of the preferred label $\pi_\theta(y_w|x)$ and decrease the probability of the dispreferred label $\pi_\theta(y_l|x)$, the term $h_{\pi_\theta}(y_w, y_l, x)$ is positive.

Lemma 3.1 *Under the assumption that the text encoder is frozen, i.e., $\mathcal{T}_{\text{ref}} = \mathcal{T}_\theta = \mathcal{T}$, the policy ratio for models using the contrastive learning policy, in the methods such as DPO or IPO can be expressed as:*

$$h_{\pi_\theta}(y_w, y_l, x) = \frac{1}{\mathcal{T}} (\mathcal{I}_\theta(x) - \mathcal{I}_{\text{ref}}(x))^T (\mathcal{T}(y_w) - \mathcal{T}(y_l)). \quad (9)$$

The proof is provided in Appendix B.1.

Based on Lemma 3.1, the term h_{π_θ} depends only on the term $(\mathcal{I}_\theta(x) - \mathcal{I}_{\text{ref}}(x))^T (\mathcal{T}(y_w) - \mathcal{T}(y_l))$. This indicates that the loss objective is designed to adjust $\mathcal{I}_\theta(x)$ to align more closely with the preferred text embedding difference, i.e., $\mathcal{T}(y_w) - \mathcal{T}(y_l)$, while maintaining appropriate proximity to the reference embedding $\mathcal{I}_{\text{ref}}(x)$. Having this in mind, we now raise the following question:

How does the Gradient update work in case of DPO/IPO?

First, we need to formulate the gradient of loss correctly in order to analyze it. The following Corollary provides a more insightful way of writing the gradient.

Corollary 3.2 *Using Lemma 3.1 we can obtain the gradient of the loss as the following. Further details is provided in Appendix B.3.*

$$\nabla_\theta \mathcal{L}_{\text{pref}}(\pi_\theta, \pi_{\text{ref}}) = - \underbrace{w_{\text{pref}}(y_w, y_l; x)}_{(I)} \cdot \underbrace{\left[\frac{\partial \mathcal{I}_\theta}{\partial \theta} \right]^T}_{(II)} (\mathcal{T}(y_w) - \mathcal{T}(y_l)), \quad (10)$$

where the *gradient weight* (I) in DPO is $w_{\text{pref}}(y_w, y_l; x) = \sigma(-\beta h_{\pi_\theta}(y_w, y_l, x))$, and in IPO, $w_{\text{pref}}(y_w, y_l; x) = \left(\frac{1}{2\beta} - h_{\pi_\theta}(y_w, y_l, x) \right)$. Intuitively, the term (II) shows that adjusting the image embedding $\mathcal{I}_\theta(x)$ in the direction of $\mathcal{T}(y_w) - \mathcal{T}(y_l)$, also encourages the model to better align with the preferred outputs. Importantly, if the distribution of π_θ deviates significantly from the reference distribution π_{ref} , the absolute value of the *policy ratio* increases. As noted previously, this effect reduces the update rate in the direction of (II), acting as a mechanism to control the model and keep it closer to the reference policy, preventing excessive divergence from the reference distribution.

In the KTO method, since there is no direct comparison between y_w and y_l , we do not get the same equation as in 9. However, the main idea still applies. The model adjusts the image embedding $\mathcal{I}_\theta(x)$ to match human preferences, but it does so through a different optimization approach.

3.3.1 REGULARIZATION

In all of our training methods, we explicitly constrain our model to be proximal to the reference model on the preference dataset $\mathcal{D}_{\text{pref}}$. However, the preference dataset $\mathcal{D}_{\text{pref}}$ is often tiny and often fails to capture the entire data manifold since, in many cases, it only contains adversarial samples and out-of-distribution samples; this leads us to introduce additional regularization terms to our training, which serve to maintain proximity between the trained model and the reference.

This motivates the introduction of a regularization term \mathcal{L}_{reg} , designed to maintain proximity between the trained model π_θ and the reference model π_{ref} as follow:

$$\mathcal{L}_{\text{reg}}(\pi, \pi_{\text{ref}}; \mathcal{D}_{\text{reg}}) = D_{\text{KL}}(\pi(y|x) || \pi_{\text{ref}}(y|x)) = \mathbb{E}_{x \sim \mathcal{D}_{\text{reg}}} \mathbb{E}_{y \sim \pi(y|x)} \left[\log \frac{\pi(y|x)}{\pi_{\text{reg}}(y|x)} \right], \quad (11)$$

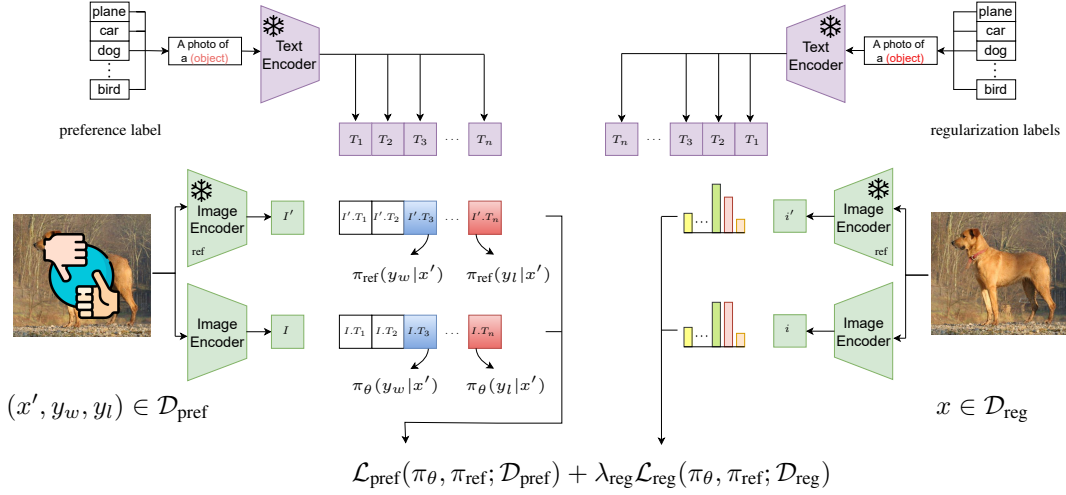


Figure 1: Overview of our proposed framework, on the left side, we calculate the preference optimization loss $\mathcal{L}_{\text{pref}}(\pi_{\theta}, \pi_{\text{ref}}; \mathcal{D}_{\text{pref}})$ using the preference dataset, and the output logits $\mathcal{T}(y_w)^T \mathcal{I}(x), \mathcal{T}(y_l)^T \mathcal{I}(x)$ from both models. on the right side the regulatory loss $\mathcal{L}_{\text{reg}}(\pi_{\theta}, \pi_{\text{ref}}; \mathcal{D}_{\text{reg}})$ is calculated using the clean regularization dataset.

where \mathcal{D}_{reg} is the set of clean images; for example, in the typographic attack task, we construct \mathcal{D}_{reg} using clean images from the training dataset. By adding this term to the loss function, the model can better maintain its accuracy on true labels, even when facing adversarial challenges, by using the regularization dataset \mathcal{D}_{reg} to ensure robustness.

A shortcoming from these preference losses also suggests us to introduce additional regularization terms.

From this point on, for the sake of simplicity, we denote $\frac{\pi_{\theta}(y_w|x)}{\pi_{\text{ref}}(y_w|x)} = x_1$ and $\frac{\pi_{\theta}(y_l|x)}{\pi_{\text{ref}}(y_l|x)} = x_2$.

In order to better understand the effect of regularization, we will build up on top of following theorem.

Theorem 3.3 (Feng et al., 2024) *The partial derivatives of Equation 5 with respect to x_1 and x_2 are given by:*

$$\left| \frac{\partial \mathcal{L}_{\text{DPO}}(x_1; x_2)}{\partial x_1} / \frac{\partial \mathcal{L}_{\text{DPO}}(x_1; x_2)}{\partial x_2} \right| = \frac{x_2}{x_1} < 1. \quad (12)$$

We also find a similar result in the case of IPO, We leave the proof in Appendix B.2.:

Proposition 3.4 *The partial derivatives of Equation 6 with respect to x_1 and x_2 are given by:*

$$\left| \frac{\partial \mathcal{L}_{\text{IPO}}(x_1; x_2)}{\partial x_1} / \frac{\partial \mathcal{L}_{\text{IPO}}(x_1; x_2)}{\partial x_2} \right| = \frac{x_2}{x_1} < 1.$$

In our problem formulation in section 3.1, we define the true label as y_w and the adversarial label (e.g., typographic label) as y_l . According to Theorem 3.3 and Proposition 3.4, the rate of increase in the probability of the preferred response y_w is lower than the rate of decrease in the probability of the dispreferred response y_l . Therefore, as suggested by Feng et al. (2024), our model primarily focuses on reducing the likelihood of the dispreferred response. This also motivates us to introduce more regulatory terms to ensure proximity.

For training, we propose using a total loss function from the dataset $\mathcal{D} = (\mathcal{D}_{\text{pref}}, \mathcal{D}_{\text{reg}})$ as follows, where \mathcal{L}_{reg} is the regularization loss and $\mathcal{L}_{\text{pref}}$ is the preference optimization objective:

$$\mathcal{L}(\pi_{\theta}, \pi_{\text{ref}}; \mathcal{D}) = \mathcal{L}_{\text{pref}}(\pi_{\theta}, \pi_{\text{ref}}; \mathcal{D}_{\text{pref}}) + \lambda_{\text{reg}} \mathcal{L}_{\text{reg}}(\pi_{\theta}, \pi_{\text{ref}}; \mathcal{D}_{\text{reg}}). \quad (13)$$

For example, consider giving images as input to CLIP, where the model chooses the corresponding caption from a fixed caption set. The selection process follows the policy we defined, using the softmax function over the similarity scores between the image and each caption in the set, as shown in Figure 1.

3.4 LINEAR TRANSFORMATIONS AND ADAPTATIONS

In many cases, fine-tuning the entire model may be unnecessary and require more interpretation and control. Therefore, we employ a linear head on top of the encoders. This linear projection layer offers a more interpretable approach, providing a plug-and-play framework where the projection can be learned during training and then applied as needed.

This linear layer also introduces a linear-algebraic perspective to the adaptation process. Suppose the learned transformation is represented by the learnable matrix W . This matrix transforms both vectors $\mathcal{I}(x)$ and $\mathcal{T}(y)$ to $W\mathcal{I}(x)$ and $W\mathcal{T}(y)$ respectively, thereby transforming the similarity function $f(y, x) = \mathcal{I}(x)^T \mathcal{T}(y) / \tau$ into a new function $\tilde{f}(y, x) = \mathcal{I}(x)^T W^T W \mathcal{T}(y) / \tau$. Utilizing the Singular Value Decomposition (SVD), we can express $W = U \Sigma V^T$. Therefore, we have:

$$\tilde{f}(y, x) = \mathcal{I}(x)^T W^T W \mathcal{T}(y) / \tau = (V^T \mathcal{I}(x))^T \Sigma^2 (V^T \mathcal{T}(y)) / \tau. \quad (14)$$

In this formulation, the unitary matrix V selects the important directions, and the diagonal matrix $\Sigma = \text{diag}(\sigma_1, \dots, \sigma_n)$ determines the degree of attenuation or amplification along each direction v_i . Specifically, each σ_i determines whether the corresponding direction v_i is strengthened ($\sigma_i > 1$) or weakened ($\sigma_i < 1$). Since our training process keeps the model close to the reference, each σ_i remains relatively close to 1, and the overall matrix $W^T W$ remains close to the identity matrix.

This observation allows for post-training adjustments, where we can strengthen or weaken each v_i as desired. One method for achieving this is by directly tuning each singular value σ_i using either linear interpolation or matrix powers, as follows:

$$W_t = U \Sigma^t V^T, \quad (15)$$

where $\Sigma^t = \text{diag}(\sigma_1^t, \dots, \sigma_n^t)$. This approach provides flexibility in adapting the model, enabling fine-grained control over the transformation applied to the encoded representations.

4 EXPERIMENTS AND RESULTS

In this section, we experimentally justify our method capabilities, using the CLIP model as our contrastive learning model. An explanation of the datasets we used can be found in section E.

Setup: For all experiments, we used 8 A100 GPUs, each with 40GB of memory. For the typographic attack experiments, hyperparameters such as β and λ were selected based on the ablation studies in the appendix. Specifically, we used $\beta = \lambda = 1$ for DPO, $\beta = \lambda = 0.01$ for IPO, and $\beta = 1.5$, $\lambda = 0.01$ for KTO. In disentangling gender bias, we also set $\beta = \lambda = 1$. All models were trained for three epochs with a batch size of 512. The learning rate was set to 2×10^{-5} , and we employed the Adamax optimizer with a linear warmup and a cosine scheduler, setting the warmup ratio to 0.1. We set the random seed to 0 for all experiments to ensure reproducibility.

4.1 TYPOGRAPHIC ROBUSTNESS

This section evaluates our method using the typographic attack mitigation task. We set up the problem as described, using the template "an image of a <class i >" (or a more dataset-specific template for non-generic images), designating the typographic class as the undesired outcome y_i and the original caption as the desired outcome y_w .

Baselines: We evaluate our method against the following baselines: pre-trained CLIP (Radford et al., 2021), PAINT (Ilharco et al., 2022), and Defense-prefix (Azuma & Matsui, 2023b), with results collected from (Azuma & Matsui, 2023b) for comparability. We use ImageNet-100, a 100-class subset of ImageNet (Russakovsky et al., 2015) to train the model. Typographic attack images are generated by adding misleading text labels to the original images, using open-source implementations from (Azuma & Matsui, 2023b).

Table 1: Classification accuracy results on the datasets: O (Original dataset) and T (Typographic dataset). Note that other methods’ analyses and experimental results on the ImageNet dataset were conducted on a subset called ImageNetV2 validation, which was not publicly available when these results were derived. We report the results on different datasets.

Method	ImageNet*		Caltech101		OxfordPets		StanfordCars		Flowers102		FGVCAircraft		DTD		SUN397		EuroSAT	
	O	T	O	T	O	T	O	T	O	T	O	T	O	T	O	T	O	T
CLIP	62.02	39.10	88.64	63.97	87.35	58.95	58.72	21.02	66.32	31.32	18.99	10.83	44.57	25.53	61.74	34.02	42.98	4.86
Materzynska+	54.38	44.91	80.53	74.73	75.01	63.61	40.33	15.79	51.86	34.95	13.23	8.28	36.28	33.03	51.06	39.52	37.32	16.22
PAINT	61.82	55.90	88.48	83.57	85.23	76.53	55.30	33.44	64.73	54.92	17.73	14.46	42.61	36.60	61.69	53.62	38.20	17.31
Defense-Prefix	62.48	49.83	89.28	79.54	87.22	72.86	57.47	28.64	63.82	44.12	19.26	14.49	40.64	31.60	61.41	43.50	43.85	9.85
Ours (DPO)	53.80	49.18	87.50	85.43	85.25	79.72	56.03	34.33	56.60	55.70	16.21	13.87	39.36	38.48	61.02	56.34	49.33	28.32
Ours (IPO)	47.61	42.75	85.73	83.78	85.32	80.44	53.67	35.02	54.50	52.80	17.97	15.86	40.53	39.94	61.91	58.05	46.12	43.23
Ours (KTO)	53.17	50.35	87.67	86.02	85.41	81.02	57.76	37.04	59.10	58.00	17.27	15.59	40.74	40.33	62.52	59.01	46.26	36.94
Difference	\downarrow 8.68	\downarrow 5.55	\downarrow 1.61	\downarrow 2.45	\downarrow 1.94	\downarrow 4.49	\downarrow 0.96	\downarrow 3.60	\downarrow 5.63	\downarrow 3.08	\downarrow 1.29	\downarrow 1.37	\downarrow 1.87	\downarrow 3.73	\downarrow 0.17	\downarrow 5.39	\downarrow 5.84	\downarrow 25.92

Our results, as seen in table 1, indicate that our method can effectively prevent typographic attacks with little loss of prior knowledge. In addition, we provided a qualitative analysis in Appendix C and D.

Table 2: Classification accuracy results on real typographic datasets.

Method	Materzynska	PAINT	RTA-100	Avg.
CLIP	43.27	50.00	47.20	46.82
Materzynska+	77.78	55.45	57.60	63.61
PAINT	53.22	58.18	53.60	55.00
Defense-Prefix	71.93	63.64	58.00	64.52
Ours (DPO)	78.57	57.29	60.35	65.40
Ours (IPO)	77.98	59.38	65.27	67.54
Ours (KTO)	80.36	56.25	62.19	66.27

4.1.1 CONTROL BETWEEN OPTICAL CHARACTER RECOGNITION AND OBJECT DETECTION

In this experiment, we apply linear adaptations and retrain the network, then evaluate the training results. We then interpolate between models using previously discussed linear transformation methods, varying the transformation scaling t , defined in 15 from -2.0 to 1.2 to assess performance. By doing this, we measure the effectiveness of our controlling scheme between the Optical Character Recognition (OCR) and Object Detection tasks.

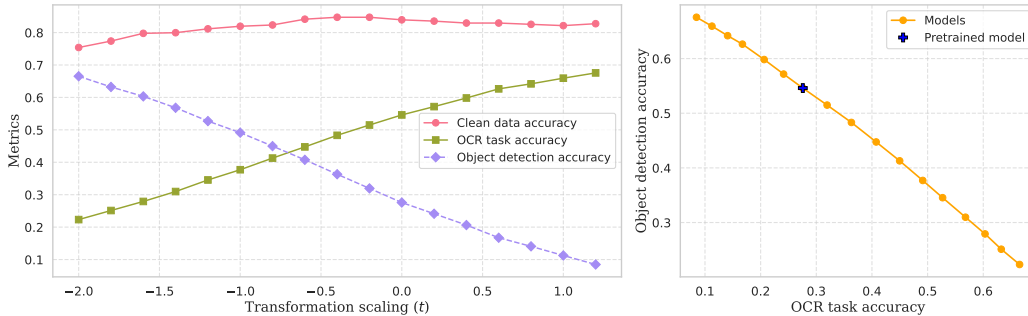


Figure 2: (Left) Accuracy on typographic samples and percentage of typographic label predictions versus transformation scaling factor t . As t increases, the model favors object labels over typographic labels while maintaining accuracy. (Right) Frontier of a DPO fine-tuned model, showing OCR accuracy vs. object detection accuracy across models with varying t .

Our results in Figure 2 demonstrate that we can confidently control the trade-off between OCR and object detection tasks without any additional training and with minimal impact on overall accuracy.

This method allows us to choose which task to prioritize flexibly, and we can visualize the performance frontier, showing that improvements in OCR accuracy come at the cost of object detection accuracy and vice versa. The ability of this linear layer to manage the trade-off suggests that the concept is linearly separable within the CLIP embedding space.

4.2 DISENTANGLING GENDER UNDERSTANDING

In this setup, we demonstrate how our approach can completely reverse a contrastive learning model’s understanding of a concept, such as gender, without significantly altering other aspects of the model’s performance.

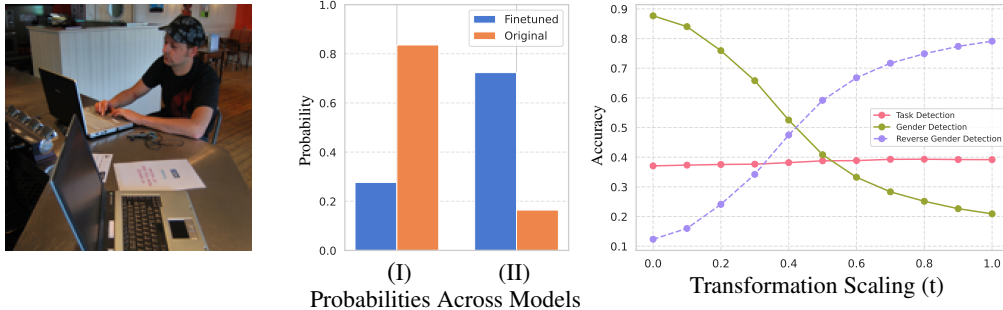


Figure 3: (Left) Image input. (Center) Comparison of model predictions before and after applying our gender-flipping method, showing changes in the predicted gender probabilities. (Right) Performance across transformation scaling t : As t increases from 0 to 1, gender-specific predictions are reversed. The intersection at t^* marks the point where gender information is effectively neutralized, leading to balanced male and female predictions. Task detection accuracy remains stable across all models. (I) and (II) are the corresponding captions: (I) The prediction that the man in the photo is working. (II) The prediction is that the woman in the photo is working.

We focus on flipping the CLIP model’s understanding of gender. We utilize a dataset of labeled images featuring men and women engaged in various activities and occupations from (Zhang et al., 2022b). The problem setup is as follows: given choices like $y_{\text{man}} = \text{"The man is <activity>"}$ and $y_{\text{woman}} = \text{"The woman is <activity>"}$, the CLIP model typically picks one of these answers. To reverse the gender understanding, we designate the label with the correct activity but flipped gender as the preferred answer y_w and the original gender-specific label as y_l .

As the regulatory term, we use the same dataset of images. However, we employ androgynous target labels such "The person in <activity>" to ensure that our model does not forget any information on detecting the correct activity. We repeat our learning process using only the linear layer and then visualize the effect of varying the transformation scaling t between 0 and 1. Our results confirm that we have a high degree of control over CLIP’s understanding of gender, as demonstrated in Figure 3.

To further evaluate our results, we apply the modified CLIP models to an image retrieval task, distinct from the original text retrieval task used for training. We assess how this impacts the retrieved images for specific text prompts by computing the similarity scores between the prompts and images as $s(\text{image}, \text{text}) = \mathcal{L}_\theta(\text{image})^T \mathcal{T}_\theta(\text{text})$. Using the dataset from (Zhang et al., 2022b), we issue prompts describing individuals in various occupations to analyze the model’s behavior and showcase an instance in Figure 4.

4.3 PRESERVING PRETRAINED KNOWLEDGE VIA PREFERENCE OPTIMIZATION

In all of the aforementioned preference optimization methods, an implicit or explicit constraint exists to keep the model as close as possible to the reference model. Specifically, including KL-divergence regularization facilitates adjustments without deviating significantly from the reference model π_{ref} . To support this claim, Figure 5-(a) shows the KL-divergence between the output distributions of the model and the reference model on the original dataset, measured as



Figure 4: Retrieved images for caption "an image of a police", Top: Reversed(6W,4M), Middle: Original(2W, 8M), Bottom: Neutralized(5W, 5M) being the model at $t = t^*$

$\mathbb{E}_{x \sim \mathcal{D}_{\text{reg}}} [D_{\text{KL}}(\pi_{\theta}(\cdot|x)|\pi_{\text{ref}}(\cdot|x))]$, after fine-tuning for the typographic robustness task using different optimization methods.

Compared to Cross-Entropy optimization, our proposed methods result in lower divergence, demonstrating better retention of the model’s pre-trained knowledge. Additionally, Figure 5-(b) illustrates that we can control this deviation (i.e., retention of pre-trained knowledge) during fine-tuning by adjusting the β hyperparameter, consistent with Equation 3. All models in (a) and (b) were trained on the *Imagenet100* and *FOOD101* datasets, respectively, and the models in (b) are optimized using the IPO method.

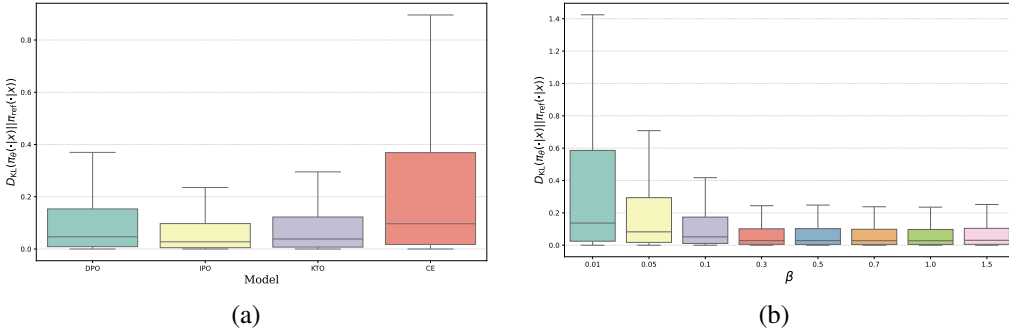


Figure 5: (a) KL-divergence comparison of our methods versus Cross-Entropy optimization. (b) Effect of the hyperparameter β on divergence between the model and reference model.

5 CONCLUSION

This paper introduced a novel framework for improving contrastive learning models through Preference Optimization (PO). Our approach systematically aligns model behavior with desired preferences, enhancing robustness against typographic attacks and effectively mitigating biases, such as gender bias, in vision-language models like CLIP. By extending techniques such as Direct Preference Optimization (DPO) and Identity Preference Optimization (IPO), we showed that preference-based optimization can fine-tune models to meet specific behavioral requirements while maintaining their pre-trained knowledge. Our experiments demonstrated improved performance over standard contrastive learning methods in adversarial robustness and fairness, particularly in handling sensitive attributes like gender and race.

This work could open new pathways for applying preference-based optimization to non-generative models. It highlights its potential for tasks requiring fairness, alignment with human values, and robustness to adversarial attacks. Future work could explore further extensions of PO to other domains and modalities and investigate more fine-grained control mechanisms for tuning model behaviors post-training.

REFERENCES

- Josh Achiam, Steven Adler, Sandhini Agarwal, Lama Ahmad, Ilge Akkaya, Florencia Leoni Aleman, Diogo Almeida, Janko Altenschmidt, Sam Altman, Shyamal Anadkat, et al. Gpt-4 technical report. *arXiv preprint arXiv:2303.08774*, 2023.
- Albert Q. Jiang, Alexandre Sablayrolles, Arthur Mensch, Chris Bamford, Devendra Singh Chaplot, Diego de las Casas, Florian Bressand, Gianna Lengyel, Guillaume Lample, Lucile Saulnier, L  lio Renard Lavaud, Marie-Anne Lachaux, Pierre Stock, Teven Le Scao, Thibaut Lavril, Thomas Wang, Timoth  e Lacroix, and William El Sayed. Mistral 7B, October 2023. URL <http://arxiv.org/abs/2310.06825>. arXiv:2310.06825 [cs].
- Mohammad Gheshlaghi Azar, Mark Rowland, Bilal Piot, Daniel Guo, Daniele Calandriello, Michal Valko, and R  mi Munos. A general theoretical paradigm to understand learning from human preferences, 2023a. URL <https://arxiv.org/abs/2310.12036>.
- Mohammad Gheshlaghi Azar, Mark Rowland, Bilal Piot, Daniel Guo, Daniele Calandriello, Michal Valko, and R  mi Munos. A General Theoretical Paradigm to Understand Learning from Human Preferences, November 2023b. URL <http://arxiv.org/abs/2310.12036>. arXiv:2310.12036 [cs, stat].
- Hiroki Azuma and Yusuke Matsui. Defense-prefix for preventing typographic attacks on clip. In *Proceedings of the IEEE/CVF International Conference on Computer Vision*, pp. 3644–3653, 2023a.
- Hiroki Azuma and Yusuke Matsui. Defense-Prefix for Preventing Typographic Attacks on CLIP, September 2023b. URL <http://arxiv.org/abs/2304.04512>. arXiv:2304.04512 [cs].
- Jiawang Bai, Kuofeng Gao, Shaobo Min, Shu-Tao Xia, Zhifeng Li, and Wei Liu. BadCLIP: Trigger-Aware Prompt Learning for Backdoor Attacks on CLIP, March 2024. URL <http://arxiv.org/abs/2311.16194>. arXiv:2311.16194 [cs].
- Yuntao Bai, Andy Jones, Kamal Ndousse, Amanda Askell, Anna Chen, Nova DasSarma, Dawn Drain, Stanislav Fort, Deep Ganguli, Tom Henighan, Nicholas Joseph, Saurav Kadavath, Jackson Kernion, Tom Conerly, Sheer El-Showk, Nelson Elhage, Zac Hatfield-Dodds, Danny Hernandez, Tristan Hume, Scott Johnston, Shauna Kravec, Liane Lovitt, Neel Nanda, Catherine Olsson, Dario Amodei, Tom Brown, Jack Clark, Sam McCandlish, Chris Olah, Ben Mann, and Jared Kaplan. Training a Helpful and Harmless Assistant with Reinforcement Learning from Human Feedback, April 2022. URL <http://arxiv.org/abs/2204.05862>. arXiv:2204.05862 [cs].
- F  bio M. Bayer, Renato J. Cintra, and Francisco Cribari-Neto. Beta seasonal autoregressive moving average models. *Journal of Statistical Computation and Simulation*, 88(15):2961–2981, July 2018. ISSN 1563-5163. doi: 10.1080/00949655.2018.1491974. URL <http://dx.doi.org/10.1080/00949655.2018.1491974>.
- Kevin Black, Michael Janner, Yilun Du, Ilya Kostrikov, and Sergey Levine. Training Diffusion Models with Reinforcement Learning, January 2024. URL <http://arxiv.org/abs/2305.13301>. arXiv:2305.13301 [cs].
- Tolga Bolukbasi, Kai-Wei Chang, James Zou, Venkatesh Saligrama, and Adam Kalai. Man is to Computer Programmer as Woman is to Homemaker? Debiasing Word Embeddings, July 2016. URL <http://arxiv.org/abs/1607.06520>. arXiv:1607.06520 [cs, stat].
- Lukas Bossard, Matthieu Guillaumin, and Luc Van Gool. Food-101–mining discriminative components with random forests. In *Computer vision–ECCV 2014: 13th European conference, zurich, Switzerland, September 6-12, 2014, proceedings, part VI 13*, pp. 446–461. Springer, 2014.
- Ralph Allan Bradley and Milton E. Terry. Rank Analysis of Incomplete Block Designs: I. The Method of Paired Comparisons. *Biometrika*, 39(3/4):324–345, 1952. ISSN 0006-3444. doi: 10.2307/2334029. URL <https://www.jstor.org/stable/2334029>. Publisher: [Oxford University Press, Biometrika Trust].

- Long Chen, Oleg Sinavski, Jan Hünermann, Alice Karnsund, Andrew James Willmott, Danny Birch, Daniel Maund, and Jamie Shotton. Driving with llms: Fusing object-level vector modality for explainable autonomous driving. In *2024 IEEE International Conference on Robotics and Automation (ICRA)*, pp. 14093–14100. IEEE, 2024.
- Paul Christiano, Jan Leike, Tom B. Brown, Miljan Martic, Shane Legg, and Dario Amodei. Deep reinforcement learning from human preferences, February 2023. URL <http://arxiv.org/abs/1706.03741>. arXiv:1706.03741 [cs, stat].
- Mircea Cimpoi, Subhansu Maji, Iasonas Kokkinos, Sammy Mohamed, and Andrea Vedaldi. Describing textures in the wild. In *Proceedings of the IEEE conference on computer vision and pattern recognition*, pp. 3606–3613, 2014.
- Kevin Clark, Paul Vicol, Kevin Swersky, and David J. Fleet. Directly Fine-Tuning Diffusion Models on Differentiable Rewards, September 2023. URL <http://arxiv.org/abs/2309.17400>. arXiv:2309.17400 [cs].
- Marcos V. Conde and Kerem Turgutlu. CLIP-Art: Contrastive Pre-training for Fine-Grained Art Classification. In *2021 IEEE/CVF Conference on Computer Vision and Pattern Recognition Workshops (CVPRW)*, pp. 3951–3955, June 2021. doi: 10.1109/CVPRW53098.2021.00444. URL <http://arxiv.org/abs/2204.14244>. arXiv:2204.14244 [cs].
- Katherine Crowson, Stella Biderman, Daniel Kornis, Dashiell Stander, Eric Hallahan, Louis Castriaco, and Edward Raff. Vqgan-clip: Open domain image generation and editing with natural language guidance. In *European Conference on Computer Vision*, pp. 88–105. Springer, 2022.
- Jia Deng, Wei Dong, Richard Socher, Li-Jia Li, Kai Li, and Li Fei-Fei. Imagenet: A large-scale hierarchical image database. In *2009 IEEE conference on computer vision and pattern recognition*, pp. 248–255. Ieee, 2009.
- Li Fei-Fei, Rob Fergus, and Pietro Perona. Learning generative visual models from few training examples: An incremental bayesian approach tested on 101 object categories. In *2004 conference on computer vision and pattern recognition workshop*, pp. 178–178. IEEE, 2004.
- Duanyu Feng, Bowen Qin, Chen Huang, Zheng Zhang, and Wenqiang Lei. Towards analyzing and understanding the limitations of dpo: A theoretical perspective, 2024. URL <https://arxiv.org/abs/2404.04626>.
- Victor Gallego. Fast Adaptation with Bradley-Terry Preference Models in Text-To-Image Classification and Generation, September 2023. URL <http://arxiv.org/abs/2308.07929>. arXiv:2308.07929 [cs].
- Saurabh Garg, Mehrdad Farajtabar, Hadi Pouransari, Raviteja Vemulapalli, Sachin Mehta, Oncel Tuzel, Vaishaal Shankar, and Fartash Faghri. TiC-CLIP: Continual Training of CLIP Models, March 2024. URL <http://arxiv.org/abs/2310.16226>. arXiv:2310.16226 [cs].
- Gabriel Goh, Nick Cammarata †, Chelsea Voss †, Shan Carter, Michael Petrov, Ludwig Schubert, Alec Radford, and Chris Olah. Multimodal Neurons in Artificial Neural Networks. *Distill*, 6(3): e30, March 2021. ISSN 2476-0757. doi: 10.23915/distill.00030. URL <https://distill.pub/2021/multimodal-neurons>.
- Ian J. Goodfellow, Jonathon Shlens, and Christian Szegedy. Explaining and harnessing adversarial examples, 2015. URL <https://arxiv.org/abs/1412.6572>.
- Patrick Helber, Benjamin Bischke, Andreas Dengel, and Damian Borth. Eurosat: A novel dataset and deep learning benchmark for land use and land cover classification. *IEEE Journal of Selected Topics in Applied Earth Observations and Remote Sensing*, 12(7):2217–2226, 2019.
- Gabriel Ilharco, Mitchell Wortsman, Samir Yitzhak Gadre, Shuran Song, Hannaneh Hajishirzi, Simon Kornblith, Ali Farhadi, and Ludwig Schmidt. Patching open-vocabulary models by interpolating weights, October 2022. URL <http://arxiv.org/abs/2208.05592>. arXiv:2208.05592 [cs].

- Jialu Wang, Yang Liu, and Xin Eric Wang. Are Gender-Neutral Queries Really Gender-Neutral? Mitigating Gender Bias in Image Search, September 2021. URL <http://arxiv.org/abs/2109.05433>. arXiv:2109.05433 [cs].
- Joanna Materzynska, Antonio Torralba, and David Bau. Disentangling visual and written concepts in CLIP, June 2022. URL <http://arxiv.org/abs/2206.07835>. arXiv:2206.07835 [cs].
- Kawin Ethayarajh, Winnie Xu, Niklas Muennighoff, Dan Jurafsky, and Douwe Kiela. KTO: Model Alignment as Prospect Theoretic Optimization, February 2024. URL <http://arxiv.org/abs/2402.01306>. arXiv:2402.01306 [cs].
- Jonathan Krause, Michael Stark, Jia Deng, and Li Fei-Fei. 3d object representations for fine-grained categorization. In *Proceedings of the IEEE international conference on computer vision workshops*, pp. 554–561, 2013.
- Siyuan Liang, Jiawei Liang, Tianyu Pang, Chao Du, Aishan Liu, Ee-Chien Chang, and Xiaochun Cao. Revisiting backdoor attacks against large vision-language models, 2024. URL <https://arxiv.org/abs/2406.18844>.
- Subhansu Maji, Esa Rahtu, Juho Kannala, Matthew Blaschko, and Andrea Vedaldi. Fine-grained visual classification of aircraft. *arXiv preprint arXiv:1306.5151*, 2013.
- Joanna Materzynska, Antonio Torralba, and David Bau. Disentangling visual and written concepts in clip, 2022. URL <https://arxiv.org/abs/2206.07835>.
- Sachit Menon, Ishaan Preetam Chandratreya, and Carl Vondrick. Task Bias in Vision-Language Models, December 2022. URL <http://arxiv.org/abs/2212.04412>. arXiv:2212.04412 [cs].
- Seyed-Mohsen Moosavi-Dezfooli, Alhussein Fawzi, and Pascal Frossard. DeepFool: a simple and accurate method to fool deep neural networks, July 2016. URL <http://arxiv.org/abs/1511.04599>. arXiv:1511.04599 [cs].
- Maria-Elena Nilsback and Andrew Zisserman. Automated flower classification over a large number of classes. In *2008 Sixth Indian conference on computer vision, graphics & image processing*, pp. 722–729. IEEE, 2008.
- Long Ouyang, Jeff Wu, Xu Jiang, Diogo Almeida, Carroll L. Wainwright, Pamela Mishkin, Chong Zhang, Sandhini Agarwal, Katarina Slama, Alex Ray, John Schulman, Jacob Hilton, Fraser Kelton, Luke Miller, Maddie Simens, Amanda Askell, Peter Welinder, Paul Christiano, Jan Leike, and Ryan Lowe. Training language models to follow instructions with human feedback, 2022a. URL <https://arxiv.org/abs/2203.02155>.
- Long Ouyang, Jeff Wu, Xu Jiang, Diogo Almeida, Carroll L. Wainwright, Pamela Mishkin, Chong Zhang, Sandhini Agarwal, Katarina Slama, Alex Ray, John Schulman, Jacob Hilton, Fraser Kelton, Luke Miller, Maddie Simens, Amanda Askell, Peter Welinder, Paul Christiano, Jan Leike, and Ryan Lowe. Training language models to follow instructions with human feedback, March 2022b. URL <http://arxiv.org/abs/2203.02155>. arXiv:2203.02155 [cs].
- Omkar M Parkhi, Andrea Vedaldi, Andrew Zisserman, and CV Jawahar. Cats and dogs. In *2012 IEEE conference on computer vision and pattern recognition*, pp. 3498–3505. IEEE, 2012.
- Alec Radford, Jong Wook Kim, Chris Hallacy, Aditya Ramesh, Gabriel Goh, Sandhini Agarwal, Girish Sastry, Amanda Askell, Pamela Mishkin, Jack Clark, Gretchen Krueger, and Ilya Sutskever. Learning Transferable Visual Models From Natural Language Supervision, February 2021. URL <http://arxiv.org/abs/2103.00020>. arXiv:2103.00020 [cs].
- Rafael Rafailov, Archit Sharma, Eric Mitchell, Stefano Ermon, Christopher D. Manning, and Chelsea Finn. Direct Preference Optimization: Your Language Model is Secretly a Reward Model, December 2023. URL <http://arxiv.org/abs/2305.18290>. arXiv:2305.18290 [cs].

- Rafael Rafailov, Archit Sharma, Eric Mitchell, Stefano Ermon, Christopher D. Manning, and Chelsea Finn. Direct preference optimization: Your language model is secretly a reward model, 2024. URL <https://arxiv.org/abs/2305.18290>.
- Gabriele Ruggeri and Debora Nozza. A Multi-dimensional study on Bias in Vision-Language models. In Anna Rogers, Jordan Boyd-Graber, and Naoaki Okazaki (eds.), *Findings of the Association for Computational Linguistics: ACL 2023*, pp. 6445–6455, Toronto, Canada, July 2023. Association for Computational Linguistics. doi: 10.18653/v1/2023.findings-acl.403. URL <https://aclanthology.org/2023.findings-acl.403>.
- Olga Russakovsky, Jia Deng, Hao Su, Jonathan Krause, Sanjeev Satheesh, Sean Ma, Zhiheng Huang, Andrej Karpathy, Aditya Khosla, Michael Bernstein, Alexander C. Berg, and Li Fei-Fei. ImageNet Large Scale Visual Recognition Challenge, January 2015. URL <http://arxiv.org/abs/1409.0575>. arXiv:1409.0575 [cs].
- Chitwan Saharia, William Chan, Saurabh Saxena, Lala Li, Jay Whang, Emily Denton, Seyed Kammar Seyed Ghasemipour, Burcu Karagol Ayan, S. Sara Mahdavi, Rapha Gontijo Lopes, Tim Salimans, Jonathan Ho, David J Fleet, and Mohammad Norouzi. Photorealistic text-to-image diffusion models with deep language understanding, 2022. URL <https://arxiv.org/abs/2205.11487>.
- Yang Shu, Xingzhuo Guo, Jialong Wu, Ximei Wang, Jianmin Wang, and Mingsheng Long. Clipood: Generalizing clip to out-of-distributions, 2023. URL <https://arxiv.org/abs/2302.00864>.
- Nisan Stiennon, Long Ouyang, Jeff Wu, Daniel M. Ziegler, Ryan Lowe, Chelsea Voss, Alec Radford, Dario Amodei, and Paul Christiano. Learning to summarize from human feedback, February 2022. URL <http://arxiv.org/abs/2009.01325>. arXiv:2009.01325 [cs].
- Zhiqing Sun, Sheng Shen, Shengcao Cao, Haotian Liu, Chunyuan Li, Yikang Shen, Chuang Gan, Liang-Yan Gui, Yu-Xiong Wang, Yiming Yang, Kurt Keutzer, and Trevor Darrell. Aligning Large Multimodal Models with Factually Augmented RLHF, September 2023. URL <http://arxiv.org/abs/2309.14525>. arXiv:2309.14525 [cs].
- Hugo Touvron, Thibaut Lavril, Gautier Izacard, Xavier Martinet, Marie-Anne Lachaux, Timothée Lacroix, Baptiste Rozière, Naman Goyal, Eric Hambro, Faisal Azhar, Aurelien Rodriguez, Armand Joulin, Edouard Grave, and Guillaume Lample. LLaMA: Open and Efficient Foundation Language Models, February 2023. URL <http://arxiv.org/abs/2302.13971>. arXiv:2302.13971 [cs].
- Amos Tversky. *Advances in Prospect Theory: Cumulative Representation of Uncertainty*, volume 5, pp. 493–519. 01 2016. ISBN 978-3-319-20450-5. doi: 10.1007/978-3-319-20451-2.24.
- Liyuan Wang, Xingxing Zhang, Hang Su, and Jun Zhu. A Comprehensive Survey of Continual Learning: Theory, Method and Application, January 2023. URL <https://arxiv.org/abs/2302.00487v3>.
- Jianxiong Xiao, Krista A Ehinger, James Hays, Antonio Torralba, and Aude Oliva. Sun database: Exploring a large collection of scene categories. *International Journal of Computer Vision*, 119: 3–22, 2016.
- Mengde Xu, Zheng Zhang, Fangyun Wei, Yutong Lin, Yue Cao, Han Hu, and Xiang Bai. A simple baseline for open-vocabulary semantic segmentation with pre-trained vision-language model, 2022. URL <https://arxiv.org/abs/2112.14757>.
- Yi Zhang, Junyang Wang, and Jitao Sang. Counterfactually measuring and eliminating social bias in vision-language pre-training models. In *Proceedings of the 30th ACM International Conference on Multimedia*, pp. 4996–5004, 2022a.
- Yi Zhang, Junyang Wang, and Jitao Sang. Counterfactually Measuring and Eliminating Social Bias in Vision-Language Pre-training Models, July 2022b. URL <http://arxiv.org/abs/2207.01056>. arXiv:2207.01056 [cs].

Yiwu Zhong, Jianwei Yang, Pengchuan Zhang, Chunyuan Li, Noel Codella, Liunian Harold Li, Luowei Zhou, Xiyang Dai, Lu Yuan, Yin Li, and Jianfeng Gao. RegionCLIP: Region-based Language-Image Pretraining, December 2021. URL <http://arxiv.org/abs/2112.09106>. arXiv:2112.09106 [cs].

Appendix

Table of Contents

A Theoretical Foundations of RLHF	17
A.1 Deriving Preference Optimization as a Supervised Learning Framework	17
B Proofs	19
B.1 Proof of Lemma 3.1	19
B.2 Proof of Proposition 3.4	19
B.3 The Gradient of the DPO and IPO Objectives	20
C What features does our method learn	20
D Latent visualization using VQGAN	20
E Datasets	20
F Hyperparameter Sensitivity Analysis	22
F.1 Effect of β	22
F.2 Ablation Study on the Regularization Loss \mathcal{L}_{reg} and the Effect of λ	23
G Beta Moving Average vs. Exponential Moving Average	23
H Sample Efficiency Analysis	24
H.1 Impact of Number of Typographic Instances per Image	25

A THEORETICAL FOUNDATIONS OF RLHF

RLHF extends the traditional reinforcement learning paradigm by incorporating human preferences into the learning process (Ouyang et al., 2022a). This feedback can take the form of direct preference comparisons between different actions or sequences of actions, or it can involve explicit corrections when the agent’s behavior is undesirable. Human judgments are converted into a reward signal that helps the agent refine its policy. RLHF has gained attention in areas like natural language processing and fine-tuning large language models, where specifying a clear reward function is difficult and aligning the agent’s behavior with human values or intentions is critical. This method offers a more robust approach to training AI systems in tasks that require subjective judgment or nuanced decision-making.

In the context of aligning Large Language Models (LLMs), RLHF plays a crucial role. The process usually begins with supervised fine-tuning (SFT) of a pre-trained model on task-specific datasets, which helps the model learn to generate appropriate responses for various queries, resulting in a reference model denoted as π_{ref} . This model is refined using RLHF, which consists of three core steps.

1. *Supervised Fine-tuning (SFT)*: Pre-trained language models often require an initial supervised fine-tuning phase to follow human instructions better. This phase aligns the model’s responses with human expectations. After this phase, we obtain a model $\pi_{\theta}^{\text{SFT}}$, which serves as the initial policy for further training.

2. *Reward Model Training*: Once the SFT model is trained, the next step in RLHF is to train a reward model $r_{\psi}(x, y)$, where x is an input prompt and y is the corresponding response. The reward model is trained to reflect human preferences between different responses. Given two responses y_w (preferred, or "win") and y_l (less preferred, or "lose"), the Bradley-Terry model is commonly used to model human preferences:

$$p^*(y_w \succ y_l | x) = \frac{e^{r_{\psi}(x, y_w)}}{e^{r_{\psi}(x, y_w)} + e^{r_{\psi}(x, y_l)}}, \quad (16)$$

which can be rewritten as:

$$p^*(y_w \succ y_l | x) = \sigma(r_{\psi}(x, y_w) - r_{\psi}(x, y_l)), \quad (17)$$

where σ is the sigmoid function. To train the reward model, the following log-loss function is minimized over a dataset of human preferences $\mathcal{D} = \{(x^{(i)}, (y_w^{(i)}, y_l^{(i)}))\}_{i=1}^N$:

$$-\mathbb{E}_{(x, y_w, y_l) \sim \mathcal{D}} [\log \sigma(r_{\psi}(x, y_w) - r_{\psi}(x, y_l))]. \quad (18)$$

3. *Fine-tuning with Reinforcement Learning*: In the final stage of RLHF, the trained reward model is kept fixed, and the policy π_{θ}^{RL} (initialized from $\pi_{\theta}^{\text{SFT}}$) is fine-tuned using the PPO algorithm. The goal is to optimize the policy to maximize the expected reward predicted by the reward model while maintaining closeness to the supervised fine-tuned model through Kullback-Leibler (KL) divergence regularization. The optimization problem is formalized as:

$$\max_{\theta} \mathbb{E}_{x \sim \mathcal{D}, y \sim \pi_{\theta}^{\text{RL}}(y|x)} [r_{\psi}(x, y) - \beta D_{\text{KL}}(\pi_{\theta}^{\text{RL}}(y|x) \parallel \pi_{\theta}^{\text{SFT}}(y|x))], \quad (19)$$

where $D_{\text{KL}}(\pi_{\theta}^{\text{RL}}(y|x) \parallel \pi_{\theta}^{\text{SFT}}(y|x))$ represents the KL divergence between the RL policy and the SFT policy. The coefficient β controls the trade-off between encouraging exploration and maintaining consistency with the supervised model. L divergence serves two purposes: it acts as an entropy bonus, encourages exploration, and ensures that the RL policy stays within the supervised fine-tuned model.

This structured process ensures that LLMs are capable of solving complex tasks and remain aligned with human preferences and ethical guidelines, which is essential in applications where human values play a crucial role.

A.1 DERIVING PREFERENCE OPTIMIZATION AS A SUPERVISED LEARNING FRAMEWORK

In traditional RLHF, RL algorithms like PPO are required to optimize the policy since the reward signal is not differentiable. However, RLHF is often slow, primarily due to the need for sampling

generations, and could be more stable in practice, especially in distributed settings. As a result, recent research has focused on designing closed-form loss functions that maximize the margin between preferred and dispreferred generations. One prominent approach is Direct Preference Optimization, which has gained popularity due to its mathematical equivalence with RLHF.

Direct Preference Optimization (DPO). DPO (Rafailov et al., 2023) leverages offline preference data to directly optimize the policy without relying on reinforcement learning-based methods like PPO. DPO demonstrates that the optimal solution to Eq. 19, π_θ^* , satisfies the following equation:

$$r_\theta(x, y) = \beta \log \frac{\pi_\theta(y|x)}{\pi_{\text{ref}}(y|x)} + \beta \log Z(x). \quad (20)$$

Here, r_θ represents the reward model, π_θ is the policy model, and π_{ref} is the reference model. Both π_θ and π_{ref} are initialized from the same SFT (Supervised Fine-Tuning) model, but only π_θ is further optimized during DPO, while π_{ref} remains unchanged. $Z(x)$ is the partition function, and β is a hyper-parameter that controls the intensity of the reward signal.

The preference probability P_θ is derived from pairwise comparisons using the Bradley-Terry model. Substituting Equation 20 into Equation 18 yields the following loss function for DPO:

$$\mathcal{L}_{\text{dpo}}(\pi_\theta; \pi_{\text{ref}}) = -\mathbb{E}_{(x, y_w, y_l) \sim \mathcal{D}} \left[\log \sigma \left(\beta \log \frac{\pi_\theta(y_w|x)}{\pi_{\text{ref}}(y_w|x)} - \beta \log \frac{\pi_\theta(y_l|x)}{\pi_{\text{ref}}(y_l|x)} \right) \right]. \quad (21)$$

In Equation 21, σ denotes the sigmoid function, and \mathcal{D} represents the dataset consisting of pairwise preferences. Each preference triplet (x, y_w, y_l) includes a prompt x , a preferred response y_w , and a less preferred response y_l . This formulation allows DPO to optimize directly on pairwise preference data, avoiding the instability of RL methods while maintaining mathematical equivalence with traditional RLHF.

Identity Preference Optimization (IPO). As the original DPO loss function has shown limitations in practice, such as overfitting to the preference dataset (Azar et al., 2023a), IPO was proposed as an extension. IPO introduces a regularization term to the DPO loss to mitigate overfitting by controlling the gap between the log-likelihood ratios of the preferred and dispreferred outputs for both the model and the reference model. The IPO loss function is defined as:

$$\mathcal{L}_{\text{IPO}}(\pi_\theta; \pi_{\text{ref}}) = -\mathbb{E}_{(x, y_w, y_l) \sim \mathcal{D}} \left[\left(\log \left(\frac{\pi_\theta(y_w|x)\pi_{\text{ref}}(y_l|x)}{\pi_\theta(y_l|x)\pi_{\text{ref}}(y_w|x)} \right) - \frac{\beta^{-1}}{2} \right)^2 \right]. \quad (22)$$

By adding this regularization, IPO ensures better generalization of the model, avoiding overfitting to specific preference patterns and maintaining stability in performance across different datasets.

Kahneman-Tversky Optimization (KTO). In language modeling, collecting large-scale preference datasets can be difficult, but it is relatively easier to determine whether an output is desirable or undesirable. This challenge has inspired KTO (Kawin Ethayarajh et al., 2024), a method that bypasses the need for detailed preference data by using a binary signal to guide optimization. KTO is based on prospect theory (Tversky, 2016), directly maximizing the utility of generations using a model of human decision-making.

KTO has demonstrated higher data efficiency and better handling of imbalanced datasets compared to DPO. The KTO loss function is defined as:

$$\mathcal{L}_{\text{KTO}}(\pi_\theta, \pi_{\text{ref}}) = \mathbb{E}_{x, y \sim \mathcal{D}} [w(y)(1 - v_{\text{KTO}}(x, y; \beta))], \quad (23)$$

where $v_{\text{KTO}}(x, y; \beta)$ adjusts based on whether the output is desirable or not:

$$v_{\text{KTO}}(x, y; \beta) = \begin{cases} \sigma(r_{\text{KTO}}(x, y) - z_{\text{ref}}) & y \sim y_{\text{desired}}|x \\ \sigma(z_{\text{ref}} - r_{\text{KTO}}(x, y)) & y \sim y_{\text{undesired}}|x \end{cases}, \quad w(y) = \begin{cases} \lambda_U & y \sim y_{\text{undesired}}|x \\ \lambda_D & y \sim y_{\text{desired}}|x \end{cases}.$$

Here, z_{ref} represents the reference reward, and $r_{\text{KTO}}(x, y) = \beta \log \frac{\pi_\theta(y|x)}{\pi_{\text{ref}}(y|x)}$. The weighting function $w(y)$ differentiates between desirable and undesirable outputs, where λ_D and λ_U are hyper-parameters controlling the weighting of each.

KTO’s key advantage is its ability to focus on maximizing the reward for desirable outputs without inflating the KL divergence term, effectively balancing utility and regularization. This makes KTO a practical solution for real-world applications, where collecting detailed preference data is infeasible.

In all three methods—DPO, IPO, and KTO—the policy π_θ is directly optimized without the need for a reward model. We incorporate these methods into our experiments to compare their effectiveness in various aspects, such as reducing bias and improving adversarial robustness and overall model performance.

B PROOFS

For simplicity, in all the sections that follow, we assume $\tau = 1$.

B.1 PROOF OF LEMMA 3.1

As seen in DPO and IPO, for preference optimization, using a preference dataset the key objective is to optimize based on a preference dataset by calculating $h_{\pi_\theta}(y_w, y_l, x)$ define in 4. using our defined policy π_θ with the softmax output, we find the following;

$$\begin{aligned} h_{\pi_\theta}(y_w, y_l, x) &= \log \left(\frac{\pi_\theta(y_w|x)\pi_{\text{ref}}(y_l|x)}{\pi_\theta(y_l|x)\pi_{\text{ref}}(y_w|x)} \right) = \log \left(\frac{\frac{e^{f_\theta(y_w, x)}}{\sum_{y_i} e^{f_\theta(y_i, x)}} \cdot \frac{e^{f_{\text{ref}}(y_l, x)}}{\sum_{y_i} e^{f_{\text{ref}}(y_i, x)}}}{\frac{e^{f_\theta(y_l, x)}}{\sum_{y_i} e^{f_\theta(y_i, x)}} \cdot \frac{e^{f_{\text{ref}}(y_w, x)}}{\sum_{y_i} e^{f_{\text{ref}}(y_i, x)}}} \right) \\ &= \log \left(e^{f_\theta(y_w, x) - f_\theta(y_l, x) + f_{\text{ref}}(y_l, x) - f_{\text{ref}}(y_w, x)} \right) \\ &= f_\theta(y_w, x) - f_\theta(y_l, x) + f_{\text{ref}}(y_l, x) - f_{\text{ref}}(y_w, x) \\ &= (\mathcal{I}_\theta(x)^T \mathcal{T}_\theta(y_w) - \mathcal{I}_\theta(x)^T \mathcal{T}_\theta(y_l) - \mathcal{I}_{\text{ref}}(x)^T \mathcal{T}_{\text{ref}}(y_w) + \mathcal{I}_{\text{ref}}(x)^T \mathcal{T}_{\text{ref}}(y_l)) / \tau \\ &= \mathcal{I}_\theta(x)^T (\mathcal{T}_\theta(y_w) - \mathcal{T}_\theta(y_l)) - \mathcal{I}_{\text{ref}}(x)^T (\mathcal{T}_{\text{ref}}(y_w) - \mathcal{T}_{\text{ref}}(y_l)). \end{aligned} \quad (24)$$

Assuming the text encoder \mathcal{T}_θ is frozen, such that $\mathcal{T}_\theta = \mathcal{T}_{\text{ref}} = \mathcal{T}$, the expression simplifies to:

$$h_{\pi_\theta}(y_w, y_l, x) = (\mathcal{I}_\theta(x) - \mathcal{I}_{\text{ref}}(x))^T (\mathcal{T}(y_w) - \mathcal{T}(y_l)). \quad (25)$$

Our loss functions aim to increase $h_{\pi_\theta}(y_w, y_l, x)$, starting from the initialized value of 0 (since π_θ is initially set to π_{ref}). With some proximity constraints, as in DPO and IPO:

$$\mathcal{L}_{\text{DPO}}(\pi_\theta, \pi_{\text{ref}}) = \mathbb{E}_{(x, y_l, y_w) \sim \mathcal{D}} [-\log \sigma(\beta h_{\pi_\theta}(y_w, y_l, x))], \quad (26)$$

$$\mathcal{L}_{\text{IPO}}(\pi_\theta; \pi_{\text{ref}}) = \mathbb{E}_{(x, y_w, y_l) \sim \mathcal{D}} \left[\left(h_{\pi_\theta}(y_w, y_l, x) - \frac{\beta^{-1}}{2} \right)^2 \right]. \quad (27)$$

B.2 PROOF OF PROPOSITION 3.4

By rewriting $\mathcal{L}_{\text{IPO}}(\pi_\theta, \pi_{\text{ref}})$ with x_1 and x_2 , we obtain:

$$\begin{aligned} \mathcal{L}_{\text{IPO}}(\pi_\theta, \pi_{\text{ref}}) &= \mathbb{E}_{(x_1, y_1, y_2) \sim \mathcal{D}} \left[\left(h_{\pi_\theta}(y_1, y_2, x_1, x_2) - \frac{\beta^{-1}}{2} \right)^2 \right] \\ &= \mathbb{E}_{(x_1, y_1, y_2) \sim \mathcal{D}} \left[\left(\log \left(\frac{x_1}{x_2} \right) - \frac{\beta^{-1}}{2} \right)^2 \right] \end{aligned} \quad (28)$$

For $\frac{\partial \mathcal{L}_{\text{IPO}}(x_1; x_2)}{\partial x_1}$,

$$\begin{aligned} \frac{\partial \mathcal{L}_{\text{IPO}}(x_1; x_2)}{\partial x_1} &= 2 \left(\log \left(\frac{x_1}{x_2} \right) - \frac{\beta^{-1}}{2} \right) \cdot \frac{1}{x_2} \frac{x_2}{x_1} \\ &= 2 \left(\log \left(\frac{x_1}{x_2} \right) - \frac{\beta^{-1}}{2} \right) \cdot \frac{1}{x_1} \end{aligned} \quad (29)$$

For $\frac{\partial \mathcal{L}_{\text{IPO}}(x_1; x_2)}{\partial x_2}$,

$$\begin{aligned} \frac{\partial \mathcal{L}_{\text{IPO}}(x_1; x_2)}{\partial x_2} &= 2 \left(\log \left(\frac{x_1}{x_2} \right) - \frac{\beta^{-1}}{2} \right) \cdot \left(-\frac{x_1}{x_2^2} \frac{x_2}{x_1} \right) \\ &= 2 \left(\log \left(\frac{x_1}{x_2} \right) - \frac{\beta^{-1}}{2} \right) \cdot \frac{-1}{x_2} \end{aligned} \quad (30)$$

and for the second part we have:

$$\begin{aligned} \left| \frac{\partial \mathcal{L}_{\text{DPO}}(x_1; x_2)}{\partial x_1} / \frac{\partial \mathcal{L}_{\text{DPO}}(x_1; x_2)}{\partial x_2} \right| &= \frac{2 \left(\log \left(\frac{x_1}{x_2} \right) - \frac{\beta^{-1}}{2} \right) \cdot \frac{1}{x_1}}{2 \left(\log \left(\frac{x_1}{x_2} \right) - \frac{\beta^{-1}}{2} \right) \cdot \frac{1}{x_2}}, \\ &= \frac{x_2}{x_1}, \end{aligned} \quad (31)$$

and finally given that $x_1 = \frac{\pi_\theta(y_w|x)}{\pi_{\text{ref}}(y_w|x)}$ and $x_2 = \frac{\pi_\theta(y_l|x)}{\pi_{\text{ref}}(y_l|x)}$ are two probability ratios, where $\pi_\theta(y|x) \in [0, 1]$ and $\pi_{\text{ref}}(y|x) \in [0, 1]$. Assuming $\pi_{\text{ref}}(y|x)$ is the probability of the fixed reference model, we can assume $\pi_{\text{ref}}(y_w|x) = \frac{1}{a}$ and $\pi_{\text{ref}}(y_l|x) = \frac{1}{b}$, where $(a, b \geq 1)$. In this case, we have $x_1 \in [0, a]$ and $x_2 \in [0, b]$. As the DPO optimization progresses, x_1 tends to increase and x_2 tends to decrease. Consequently, $\pi_\theta(y_w|x)$ will be greater than $\frac{1}{a}$, and $\pi_\theta(y_l|x)$ will be smaller than $\frac{1}{b}$. In other words, this implies that $x_1 = \frac{\pi_\theta(y_w|x)}{\pi_{\text{ref}}(y_w|x)}$ is greater than 1, $x_2 = \frac{\pi_\theta(y_l|x)}{\pi_{\text{ref}}(y_l|x)}$ is less than 1, and therefore $x_2 < x_1$.

B.3 THE GRADIENT OF THE DPO AND IPO OBJECTIVES

The gradients of these loss functions highlight how the image encoder \mathcal{I}_θ is adjusted to align more closely with the desired output:

$$\nabla_\theta \mathcal{L}_{\text{DPO}}(\pi_\theta, \pi_{\text{ref}}) = -\beta \left[\underbrace{\sigma \left(-\beta h_{\pi_\theta}(y_w, y_l, x) \right)}_{\text{higher when proximal to reference}} \cdot \underbrace{\left[\frac{\partial \mathcal{I}_\theta}{\partial \theta} \right]^T (\mathcal{T}(y_w) - \mathcal{T}(y_l))}_{\text{increase } \mathcal{I}_\theta(x) \text{ in direction of } \mathcal{T}(y_w) - \mathcal{T}(y_l)} \right]. \quad (32)$$

$$\nabla_\theta \mathcal{L}_{\text{IPO}}(\pi_\theta, \pi_{\text{ref}}) = - \left[\underbrace{\left(\frac{\beta^{-1}}{2} - h_{\pi_\theta}(y_w, y_l, x) \right)}_{\text{positive when proximal to reference}} \cdot \underbrace{\left[\frac{\partial \mathcal{I}_\theta}{\partial \theta} \right]^T (\mathcal{T}(y_w) - \mathcal{T}(y_l))}_{\text{increase } \mathcal{I}_\theta(x) \text{ in direction of } \mathcal{T}(y_w) - \mathcal{T}(y_l)} \right]. \quad (33)$$

These gradients show that both DPO and IPO adjust the image embedding $\mathcal{I}_\theta(x)$ in the direction of $\mathcal{T}(y_w) - \mathcal{T}(y_l)$, encouraging the model to better align with the preferred outputs.

C WHAT FEATURES DOES OUR METHOD LEARN

In Figure 6, we showcase how applying our method, forces the model to focus on the suitable features of the data rather than different sorts of attacks such as typographic.

D LATENT VISUALIZATION USING VQGAN

In this section, we further investigate our fine-tuned CLIP on typographical attack datasets. We use VQGAN-CLIP (Crowson et al., 2022) as the generative model which use CLIP in its backbone. The results are shown in figure 7. As can be seen, our fine-tuned CLIP completely ignores text in its image encoder representation and only focus on visual concepts which increase it reliability and trustworthiness.

E DATASETS

Table 3 shows the statistics of the datasets we used in this paper. To evaluate the accuracy of our method on both normal classification and typographic classification (results on table 1), we consider

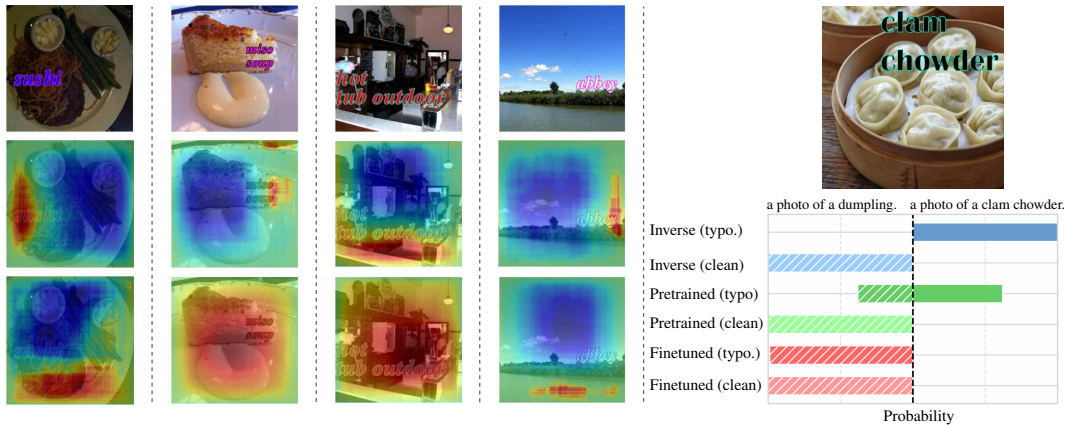


Figure 6: Typographic attack assessment. (Left) Saliency maps of vanilla CLIP and our fine-tuned version on typographic images. Each column represents a sample consisting of a typographic image, a saliency map for the prediction of vanilla CLIP, and a saliency map for the prediction of our fine-tuned version. As seen, vanilla CLIP focuses on irrelevant parts of images, especially typo texts, which results in false predictions. On the other hand, our model is capable of ignoring such fake text and focusing on the visual concept of the image, which results in true prediction. (Center) Image after typographic attack with misleading text (“clam chowder”). (Right) Model predictions: The finetuned model remains robust, correctly classifying the attacked image, while the original model misclassifies it. The inverse model confidently selects the typographic label but preserves classification accuracy.



Figure 7: Retrieved images using VQGAN-CLIP (Crowson et al., 2022). The captions for image generation is “focus”, “Love”, “Male police”, “Time”. As can be seen, vanilla CLIP put the texts on image too, but our model fine-tuned on typographical attack dataset, SUN, ignores such image texts and generated only visual concepts.

9 datasets: ImageNet-100 (Deng et al., 2009), Caltech101 (Fei-Fei et al., 2004), OxfordPets (Parkhi et al., 2012), StanfordCars (Krause et al., 2013), Flowers102 (Nilsback & Zisserman, 2008), FGVC-AirCrafts (Maji et al., 2013), DTD (Cimpoi et al., 2014), SUN397 (Xiao et al., 2016) and EuroSAT (Helber et al., 2019). These datasets are not typographic attack datasets, so we follow the procedure in (Azuma & Matsui, 2023a) to generate typographic attack images from these datasets. We also consider three more datasets designed for typographic attacks (results on table 2): Materzynska (Materzynska et al., 2022), PAINT (Ilharco et al., 2022), and RTA-100 (Azuma & Matsui, 2023a). Figure 8 shows some samples from the RTA-100 dataset. Additionally, for the Gender Bias results

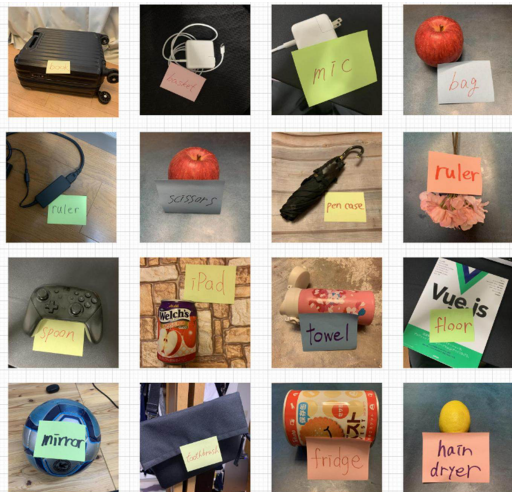


Figure 8: Samples from RTA-100 dataset.

Table 3: Datasets statistics

Dataset	Num. of. Classes	Num. of. Images
ImageNet-100	100	130,000
Caltech101	101	9,146
OxfordPets	37	7,393
StanfordCars	196	16,185
Flowers102	102	8,189
FGVCAircraft	100	10,000
DTD	47	5,640
SUN397	397	108,754
EuroSAT	10	27,000
Food101	101	101,000
Materzynska	19	171
PAINT	89	110
RTA-100	100	1,000
VL-Bias	65	24,000

and analysis, we considered the VL-Bias Zhang et al. (2022a) dataset. Also, we consider Food101 (Bossard et al., 2014) for additional experiments, including saliency maps in section C.

F HYPERPARAMETER SENSITIVITY ANALYSIS

In this section, we analyze the impact of several hyper-parameters such as β and λ . We utilize the *FOOD101* dataset for training and *SUN* as the zero-shot dataset to assess model generalization. All experiments are conducted for 3 epochs, with a learning rate of 2×10^{-5} , and a coefficient $\gamma = 0.7$ in the Beta Moving Average.

F.1 EFFECT OF β

The hyper-parameter β controls the deviation from the policy in the loss function 13. To assess its impact, we experiment with values between 0.01 and 1.5 on both the in-domain and zero-shot datasets.

As shown in Figure 9, our results indicate that IPO is highly sensitive to β . Additionally, the performance of both DPO and KTO decreases for excessively large β values on the zero-shot dataset.

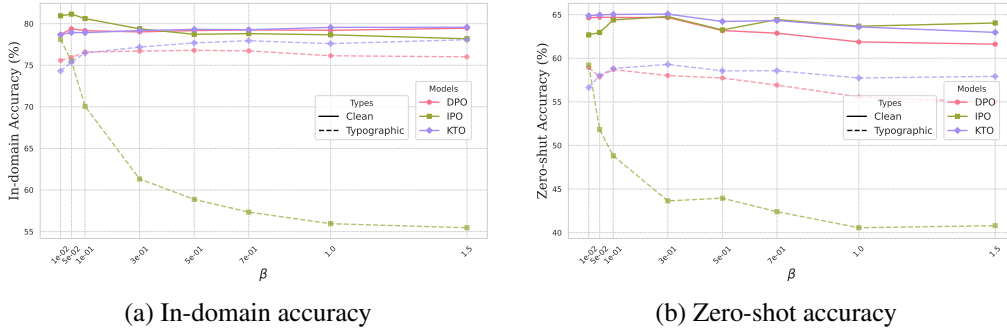


Figure 9: Ablation study on the effect of the hyper-parameter β on classification accuracies for clean and typographic datasets. The results highlight the performance of DPO, IPO, and KTO models and their impact on in-domain accuracy and (b) zero-shot accuracy.

F.2 ABLATION STUDY ON THE REGULARIZATION LOSS \mathcal{L}_{REG} AND THE EFFECT OF λ

The hyperparameter λ serves as the weight of the regularization term in our loss function. This regularizer is crucial for maintaining model performance on clean datasets during debiasing and adversarial training procedures. As shown in Figure 10, we vary λ between 0.01 and 2.0 to analyze its impact on both in-domain and zero-shot datasets, highlighting a trade-off. In the zero-shot dataset, excessively large λ values result in improved performance on the clean dataset but a decrease in performance on the typographic dataset. Conversely, very small values of λ (e.g., 0.01) lead to lower performance on the clean dataset and higher performance on the typographic dataset.

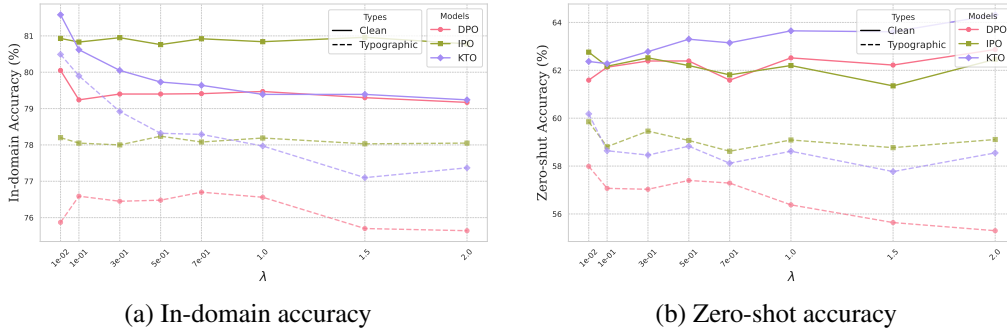


Figure 10: Ablation study on the effect of the hyper-parameter λ on classification accuracies for clean and typographic datasets. The results highlight the performance of DPO, IPO, and KTO models and their impact on in-domain accuracy and (b) zero-shot accuracy.

G BETA MOVING AVERAGE VS. EXPONENTIAL MOVING AVERAGE

Fine-tuning enhances task-specific performance but can degrade a model’s generalization, particularly in zero-shot tasks. Exponential Moving Average (EMA) tends to accelerate this degradation by diminishing the pre-trained model’s influence over time, whereas Beta Moving Average (BMA) (Bayer et al., 2018) retains more knowledge from the pre-trained model, achieving a better balance between task-specific adaptation and generalization. This balance is essential for tasks like debiasing, adversarial robustness, and zero-shot classification, as evidenced in VLMs for out-of-distribution detection (Shu et al., 2023). BMA applies a temporal ensemble approach, weighting each training checkpoint along the fine-tuning trajectory by a Beta distribution to compute the final

model state.

$$\theta^{\text{TE}} = \sum_{t=0}^T \frac{\alpha_t}{\sum_{k=0}^T \alpha_k} \cdot \theta_t, \quad (34)$$

where α_t is determined by a Beta distribution and controls how much influence each model has in the final ensemble. Unlike EMA, which rapidly diminishes the contribution of earlier models (including the pre-trained model), BMA ensures that θ_0 remains a significant part of the model’s knowledge, promoting better zero-shot generalization.

The weights α_t are drawn from the Beta distribution, normalized over the training steps:

$$\alpha_t = \text{Beta}(\gamma, \gamma) \left(\frac{t + 0.5}{T + 1} \right), \quad (35)$$

where γ is a hyper-parameter that controls the balance between the pre-trained and fine-tuned models. By setting $\gamma < 1$, we ensure that both the pre-trained and fine-tuned models contribute more heavily to the final averaged model, thus reducing the forgetting problem of EMA.

To make BMA efficient in practice, it can be implemented as a moving average:

$$\theta_t^{\text{BMA}} = \frac{\sum_{k=0}^{t-1} \alpha_k \cdot \theta_k^{\text{BMA}} + \alpha_t \cdot \theta_t}{\sum_{k=0}^t \alpha_k}, \quad (36)$$

which allows us to compute the model’s temporal ensemble without needing to store all the intermediate checkpoints.

In all of our reported results, we employed the BMA update strategy to enhance zero-shot performance. The specifics of our training procedure are detailed in Algorithm 1, where: x denotes the original image, \tilde{x} the perturbed image (e.g., typographic image), y the label, and \tilde{y} the adversarial label (e.g., typographic label). As demonstrated in Table 4, we compare the performance of BMA and EMA. The hyperparameters β and λ for each method are the same as those used during their training on ImageNet.

Algorithm 1 Preference optimization for contrastive learning with BMA details

Require: Pre-trained CLIP model π_{θ_0} , Dataset $\mathcal{D} = (\mathcal{D}_{\text{pref}}, \mathcal{D}_{\text{reg}})$, Regularization coef. λ_{reg} , learning rate η

- 1: Initialize BMA model: $\theta_0^{\text{BMA}} \leftarrow \text{detach}(\theta_0)$
- 2: Initialize policy: $\theta_0^\pi \leftarrow \theta_0$
- 3: **for** $t = 1$ to T **do**
- 4: $b_{\text{pref}}, b_{\text{reg}} \leftarrow b = \{(x, y, \tilde{x}, \tilde{y})\}$ ▷ Get batch of preference / regularization data
- 5: $l_{\text{pref}} \leftarrow \mathcal{L}_{\text{po}}(\pi_{\theta_{t-1}}, \pi_{\text{ref}}; b_{\text{pref}})$ ▷ Compute preference loss using $b_{\text{pref}} = \{(\tilde{x}, y, \tilde{y})\}$
- 6: $l_{\text{reg}} \leftarrow \mathcal{L}_{\text{reg}}(\pi_{\theta_{t-1}}, \pi_{\text{ref}}; b_{\text{reg}})$ ▷ Compute regulatory loss using $b_{\text{reg}} = \{(x, \tilde{x})\}$
- 7: $l_{\text{tot}} \leftarrow l_{\text{reg}} + \lambda_{\text{reg}} \cdot l_{\text{reg}}$ ▷ Total loss
- 8: Update parameters of policy: $\theta_t^\pi \leftarrow \theta_{t-1}^\pi - \eta \nabla_{\theta_{t-1}^\pi} l_{\text{tot}}$
- 9: Calculate α_t of the current model as in Eq. 35
- 10: Update the BMA model θ_t^{BMA} as in Eq. 36
- 11: **end for**

Ensure: The final BMA model θ_T^{BMA}

where: x = Original image, \tilde{x} = Typographic image, y = Label, \tilde{y} = Typographic label

H SAMPLE EFFICIENCY ANALYSIS

In this section, we examine how efficiently our model learns with different dataset sizes. This analysis helps us understand how well the models perform with less data and how their accuracy changes as the dataset grows (see Figure 11). As expected, based on the foundation in Section 4.2 of (Azar et al., 2023a), when there is insufficient training data, DPO tends to overfit, leading to poor performance on both *In-domain* and *Zero-shot* datasets, while KTO performs better in this situation.

Specifically, we focus on the impact of the number of typographic instances per image and how this affects both the in-domain and zero-shot generalization performance.

Table 4: Comparison of the effect of BMA and EMA optimization strategies on the in-domain dataset (FOOD101) and the zero-shot dataset (SUN).

(a) In-domain accuracy					(b) Zero-shot accuracy				
Method	Original		Typographic		Method	Original		Typographic	
	BMA	EMA	BMA	EMA		BMA	EMA	BMA	EMA
CLIP	78.88		51.43		CLIP	61.00		35.33	
DPO	79.20	78.99	76.14	75.49	DPO	61.87	62.26	55.56	54.08
IPO	81.94	80.67	78.12	76.90	IPO	62.67	61.85	59.22	58.22
KTO	81.58	79.99	80.49	80.63	KTO	62.37	61.76	60.18	59.20

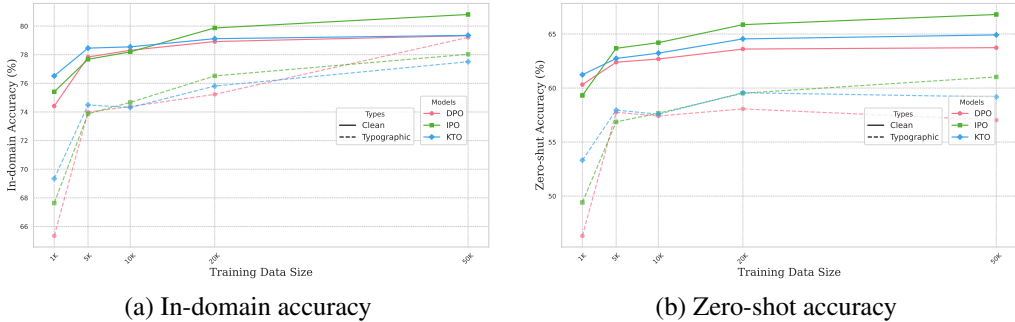


Figure 11: Ablation study on the effect of dataset size on classification accuracies for clean and typographic datasets. The results highlight the performance of DPO, IPO, and KTO models and their impact on (a) in-domain accuracy and (b) zero-shot accuracy.

Table 5: Impact of number of typographic instances per image on in-domain (FOOD101) and zero-shot (SUN) performance. Results show accuracy (%) for different settings.

Number of Instances	FOOD101 (In-domain)		SUN (Zero-shot)	
	BMA	EMA	BMA	EMA
1	74.85	75.24	58.27	57.47
3	75.22	75.25	58.83	58.46
5	75.59	75.49	58.18	58.07
10	76.25	75.78	57.88	57.29

H.1 IMPACT OF NUMBER OF TYPOGRAPHIC INSTANCES PER IMAGE

To investigate the effect of varying the number of typographic instances per image, we conducted experiments using 1, 3, 5, and 10 typographic variations for each image on the *FOOD101* dataset (in-domain) and the *SUN* dataset (zero-shot). We evaluate the effect of varying the number of typographic instances per image on model performance. The results, summarized in Table 5, suggest that increasing the number of instances does not significantly improve accuracy, indicating that this augmentation technique may not be effective for enhancing the model’s generalization.